

Telecom wavelength single-photon source based on InGaSb/AlGaSb quantum dot technology

Teemu Hakkarainen,^{1,2} Joonas Hilska,¹ Arttu Hietalahti,³ Sanna Ranta,¹ Markus Peil,¹ Emmi Kantola,³ Abhiroop Chellu,¹ Efsane Sen,¹ Jussi-Pekka Penttinen,³ Mircea Guina¹*

¹ Optoelectronics Research Centre, Physics Unit, Tampere University, FI-33720 Tampere, Finland

² Institute for Advanced Study, Tampere University, FI-33100 Tampere Finland

³ VEXLUM Oy, FI-33710 Tampere, Finland

* teemu.hakkarainen@tuni.fi Korkeakoulunkatu 3, FI33720 Tampere, Finland, +358504144134

Abstract

Deterministic light sources capable of generating quantum states on-demand at wavelengths compatible with fiber optics and atmospheric transmission are essential for practical applications in quantum communication, photonic quantum computing, and quantum metrology. To this end, single-photon emission at 1500 nm is demonstrated from an InGaSb quantum dot (QD) grown by filling droplet-etched nanoholes for the first time. The QD was embedded in a device structure comprising an antimony-based high refractive index contrast back-reflector designed for cryogenic operation and a solid immersion lens for improved photon extraction. The longitudinal optical (LO) phonon assisted excitation of the QD ground state and quasi-resonant excitation of the QD excited state is realized with a novel compact wavelength-tunable power-stabilized semiconductor laser. These direct approaches to exciting a single QD unlock access to its excitonic fine structure. The neutral exciton-biexciton structure exhibits a negative binding energy of 1.4 meV (2.6 nm) and a fine structure splitting of $24.1 \pm 0.4 \mu\text{eV}$. Furthermore, spectrally pure/isolated emission from a charged single exciton state with a single-photon purity of 95 % is achieved with LO phonon assisted two-color excitation. These results represent a major step forward for the use of the novel antimonide-based QD emitters as deterministic quantum light sources in complex quantum secure networks exploiting the wavelength compatibility with standard telecom fibers.

Introduction

Semiconductor light sources capable of generating photonic quantum states on demand are essential building blocks for applications like quantum communication,¹ quantum computing^{2,3} quantum metrology.⁴ Quantum-secure communication has already been demonstrated at system level in the BB84 scheme using InGaAs quantum dots (QDs)⁵ emitting at 920 nm and in the Ekert91 scheme using GaAs QDs emitting polarization-entangled photons at 780 nm.⁶ However, these pioneering demonstrations showcasing the capabilities of III-V semiconductor QDs for quantum key distribution are either limited to short-range fiber or free-space links⁶ or rely on non-linear frequency conversion to shift the emission to a fiber-compatible wavelength.⁵ Ultimately, QDs emitting at the wavelengths most compatible with optical fibers and atmospheric transmission windows are essential for practical applications, such as quantum communication networks combining terrestrial optical fibers and satellite links.⁷ This need has driven an active exploration of alternative QD materials emitting in the 3rd telecom window.^{8,9,10,11}

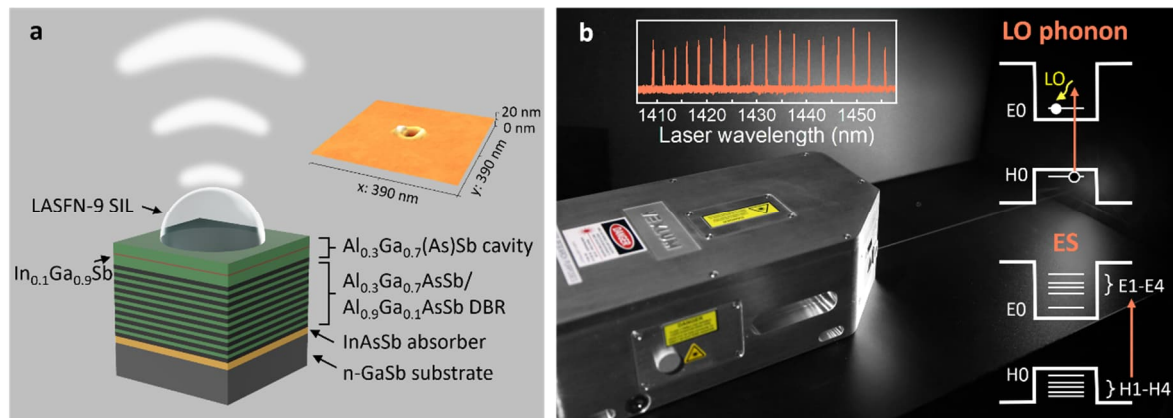
We have recently introduced a new antimonide-based QD system exhibiting narrow-linewidth excitonic emission at 1470 nm¹², formed by GaSb-filling of droplet-etched nanoholes in AlGaSb. GaAs/AlGaAs QDs emitting at 780 nm grown by the same technique have been shown to exhibit narrow exciton linewidths,¹³ extremely small inhomogeneous broadening due to size uniformity,¹⁴ bright single-photon emission,¹⁵ and vanishing fine structure splitting (FSS) owing to their dimensional symmetry and lack of strain-induced piezoelectric asymmetries.¹⁶ These characteristics have enabled their use as non-classical light sources providing state-of-the-art performance in terms of photon indistinguishability and entanglement.^{15,17,18,19} The new antimonide-based QDs have already shown several beneficial features, such as extremely homogeneous ensemble emission,¹² a suitably low QD density necessary for single-QD devices,¹² and single-photon emission in the telecom S-band.²⁰ However, the advantages of the antimonide material system has not been fully exploited. For example, the antimony system offers wide tunability of the band gap and strain, while also enabling high refractive index contrast materials for efficient photonic structures like Bragg mirrors and waveguides. Additionally, they are compatible with monolithic integration on silicon by direct epitaxial growth because the lattice mismatch between GaSb-based materials and dissimilar substrates can be relaxed right at the first interface by the formation of a network of 90°-dislocations^{21,22} and exploitation of nucleation layers.²³ These unique plastic properties have enabled epitaxial growth of mid-infrared III-Sb semiconductor lasers on Si substrates.²⁴

In recently published work, we have identified a 5 meV energy barrier for non-resonantly excited charge carriers to enter the GaSb QD from the surrounding medium.²⁵ While such a barrier can potentially protect the QD from charge fluctuations when employing coherent resonant excitation¹³ or incoherent quasi-resonant excitation,²⁶ it introduces challenges in the measurement of QD properties when employing above-band excitation. The main challenges include:

- Slow decay characteristics and volcano-shaped autocorrelation response due to delayed feeding of charge from a charge reservoir outside the QD;²⁰
- Difficulty in studying the excitonic structure of a single QD due to highly convoluted spectral properties arising from simultaneously exciting a large number of charge complexes and multiple QDs;^{12,20}
- Limited achievable photon count rate at excitation powers low enough to produce isolated exciton lines.

In this work, we introduce a single-photon emitter based on a single InGaSb/AlGaSb QD (Fig. 1a) with an indium content of 10% corresponding to emission at 1500 nm wavelength region. The QD is excited quasi-resonantly with a compact frequency-tunable single-frequency semiconductor laser (VECSEL developed by Vexlum) operating in continuous-wave regime in the 1400–1470 nm range (Fig. 1b). The laser platform has been particularly developed for atom and ion-based quantum systems^{27,28}, offering low-noise operation down to sub-Hz linewidths,²⁹ wavelength flexibility, high beam quality, and accurate frequency tuning for tens of nm over longitudinal modes and GHz-level of hop-free tuning range. Here, such laser was developed for exciting an InGaSb QD, either by quasi-resonantly pumping the excited states of the QD or by phonon-mediated pumping of the ground state transition. Consequently, for the first time, we gain access to the excitonic fine structure of InGaSb/AlGaSb QDs and their single-photon emission characteristics without the convoluted dynamics caused by charge reservoir.

Fig. 1: The single-photon source device structure and the excitation laser



a Schematic illustration of the antimonide-based QD device. The QDs, located in the middle of the AlGa(As)Sb λ -cavity, were grown by filling droplet-etched nanoholes with $\text{In}_{0.1}\text{Ga}_{0.9}\text{Sb}$. The surface profile of a nanohole is shown in the inset. The bottom mirror is a 9.5-pair AlGaAsSb distributed Bragg reflector (DBR). The device structure is separated from the substrate with an InAsSb absorber to block unwanted luminescence from the n-GaSb at the QD emission wavelength. A hemispherical solid immersion lens (SIL) is bonded on top of the semiconductor structure for enhancing photon extraction. **b** The QD device is excited with a vertical external cavity surface emitting laser (VECSEL) providing single-frequency continuous-wave operation in the range from 1400 to 1470 nm. These wavelengths allow LO phonon assisted excitation of the QD ground state (H0-E0) and quasi-resonant excitation of transitions between excited states (ES) of holes (H1-H4) and electrons (E1-E4).

Results

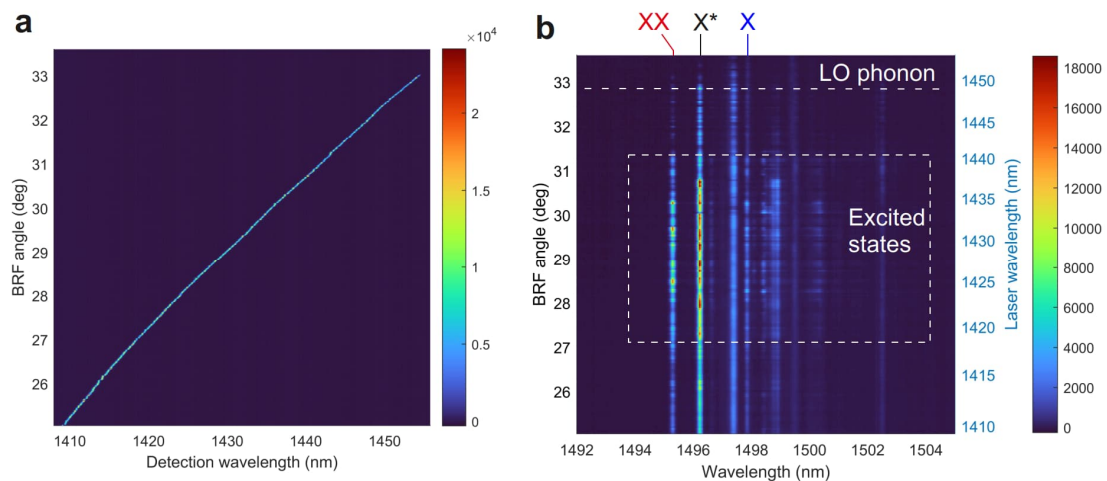
The optical experiments were carried out for InGaSb QDs embedded in the device structure presented in Fig. 1a. The device combines a Bragg mirror back-reflector and a solid immersion lens (SIL) for improving the photon collection efficiency into the available numerical aperture (NA) of the microscope objective. As explained in Supp. Info. Section 2, which deals with the optical design of the device, we expect around 16% collection efficiency for $\text{NA}=0.81$. The experimental setup is described in detail in Supp. Info. Section 4. First, we scan the birefringent filter (BRF) of the laser in order to sweep the lasing wavelength across the tuning range and record the back-reflected laser intensity as a function of wavelength. As shown in Fig. 2a, single-mode output is observed throughout the tuning range. Rotation of the BRF

allows hopping between the cavity modes with 1 GHz resolution, which is fine enough for being able to access all absorption lines of a QD. The laser locks at a lasing mode with remarkable stability; therefore, we disturb the laser by driving acoustic frequency square wave to the piezo stage connected to one of the cavity mirrors. This allows fast hopping between cavity modes without skipping.

The first step in single-QD characterization is photoluminescence excitation spectroscopy (PLE), where the QD emission spectrum in the 1500 nm range is recorded as a function of excitation wavelength. The results of the PLE scan are shown in Fig. 2b, where the intensity of the QD's excitonic emission lines are observed to vary as a function of the excitation wavelength. A broad absorption band centered at 1430 nm is observed, which is close to the wavelength where the excited states of the QD are observed in the photoluminescence (PL) spectrum of a QD ensemble (Fig. S2). Therefore, we attribute the broad absorption band to a combination of transitions between excited electron and hole states (quasi-resonant excitation). Based on the quantum mechanical model of GaSb/AlGaSb QDs²⁵, we can expect a combination of transitions between the first four excited electron and hole states in this range, with each transition having slightly different energy and strength associated with the selection rules.

At the higher end of the tuning range, we observe a narrow resonance peaking at the laser wavelength of 1449 nm. This line arises from excitation of the 1496.3 nm emission assisted by participation of a single LO phonon^{30,31} having energy of 27 meV (GaSb-like LO phonon in the Al_{0.3}Ga_{0.7}Sb barrier³²). In the following experiments we excite the QD either at the wavelength of 1435 nm (BRF 30.4°) or at 1449 nm (BRF 32.8°), which are from now onwards referred to as excited state (ES) excitation and LO phonon assisted excitation, respectively.

Fig. 2: PLE spectroscopy of a single InGaSb QD



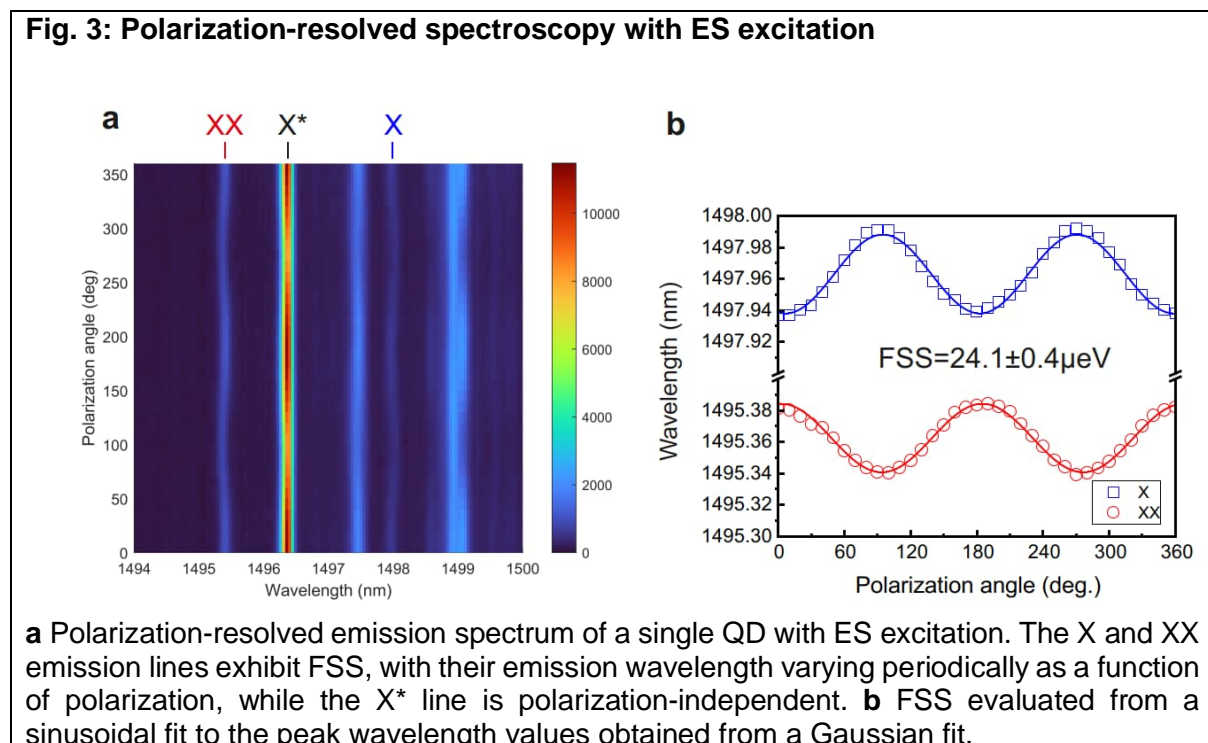
a Single-mode lasing characteristics of the frequency-tunable excitation laser. The laser spectrum was detected from the intensity reflected from the QD device. The laser wavelength is tuned by rotating a BRF inside the laser cavity. **b** PLE results for a single InGaSb QD obtained with a laser excitation power of 4 μ W maintained across different excitation wavelengths.

We proceed by recording the excitonic spectra of the QD as a function of detection polarization using ES excitation (Fig. 3). As shown in Fig. 3a, two emission lines exhibit fine structure with their peak position depending on the polarization. These lines are identified as a neutral exciton (X) at 1498.0 nm and biexciton (XX) at 1495.4 nm from power-dependent PL data

(Supp. Info. Section 6.). The dominant emission line at 1496.3 nm showing no fine structure is identified as a trion (X^*). Given the nature of native defects in antimonide materials,^{33,34} X^* is most probably positively charged. The exciton line located between X and X^* is then the negatively charged trion which shows no fine structure and has a power-dependency similar to X^* . As shown in Supp. Info (Fig. S7), we observe a competition between differently charged trions when the excitation power is changed. Noticeably, the dynamics can be shifted more in favor of the dominant X^* at 1496.3 nm by adding a 950 nm LED as a weak above-band excitation source (two-color excitation³⁵).

Now that we have, for the first time, been able to provide an overview of a single InGaSb/AlGaSb QD's spectrum and identified the different charge complexes, we can proceed to analyze the excitonic structure in more detail. A negative biexciton binding energy, $\Delta E_{XX} = E_X - E_{XX} = -1.4$ meV (-2.6 nm), is obtained from the X - XX peak separation. Similar behavior is shown for another QD Fig. S6 (Supp. Info.). The observed values of ΔE_{XX} are comparable to what is seen in GaAs/AlGaAs QDs grown by filling droplet-etched nanoholes,^{14,15,17,36} which however tend to have positive values. For the InGaSb/AlGaSb QDs investigated here, the observed negative values of ΔE_{XX} suggest a small confinement volume,³⁷ which is consistent with the energy separation between the ground state and the excited states.

A FSS of 24.1 ± 0.4 μeV is obtained from a sinusoidal fit to the XX peak position. Based on the investigation of 5 QDs, we conclude that this is a typical value for the investigated sample since we mainly observe FSS values in the 20-26 μeV range (Fig. S8. Supp. Info.), while an outlier with $\text{FSS} = 5.1 \pm 0.3$ μeV is also identified. Overall, the observed FSS values indicate that further growth optimization for improving the QD symmetry is required for reducing the FSS down to a level required for high fidelity of polarization-entanglement.



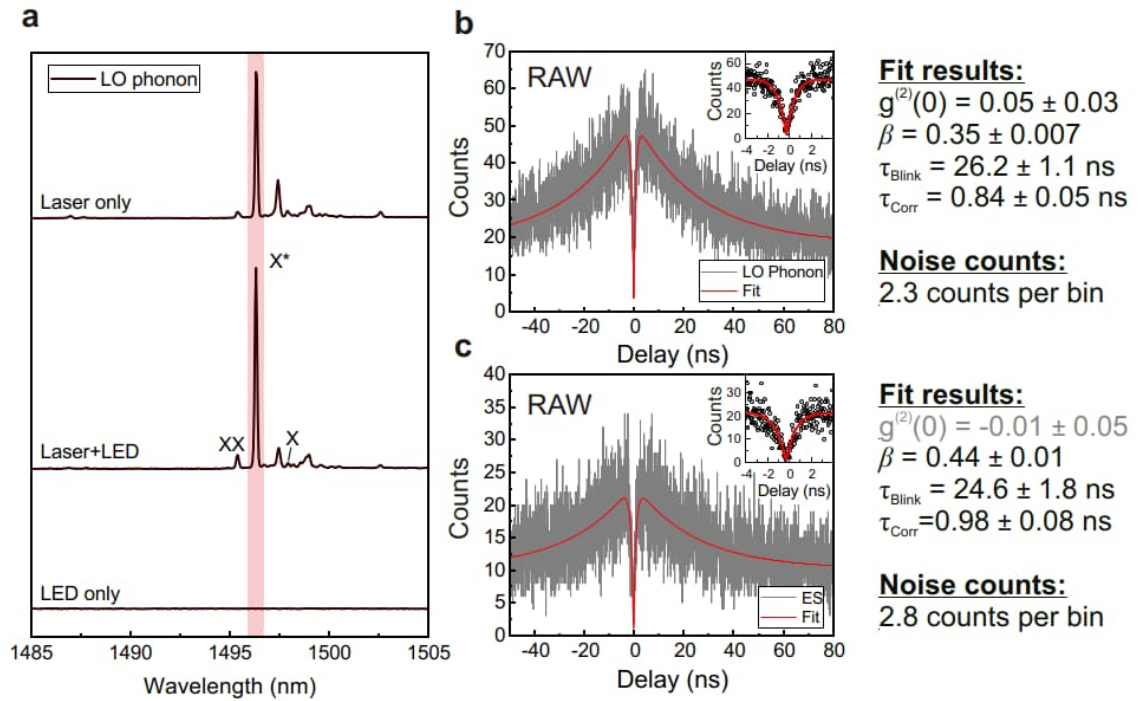
As shown in Fig. 3 and discussed above, the ES excitation scheme is effective for revealing the full excitonic structure and for investigating the fine structure of the confined states in the QD. Next, we set the laser wavelength to 1449 nm for LO phonon assisted excitation of the QD ground state. As shown in Fig. 4a, this results in an emission spectrum dominated by the

X^* transition. By implementing two-color excitation³⁸ using an additional 950 nm LED for above-band excitation of the AlGaSb barrier, we can further shift the charge dynamics in favor of X^* , with 60% of the spectrally integrated intensity now being emitted from the X^* .

Fig. 4b shows a second-order autocorrelation trace of the X^* emission line counted in a fiber-based Hanbury-Brown-Twiss configuration using two-color excitation with the laser wavelength set to the LO phonon assisted transition. The experimental data is fitted with a model including photon antibunching (single-photon emission) and spectral blinking.³⁹ We obtain a multi-photon emission probability of $g^{(2)}(0)=0.05\pm 0.03$, which compares well with the value of 0.019 ± 0.001 reported for GaAs/AlGaAs QDs with pulsed LO phonon assisted excitation³⁰ and 0.074 ± 0.004 reported for InAs QDs emitting at 1550 nm with resonant excitation.¹¹ The observed blinking characteristics are similar to the values reported in GaAs/AlGaAs QDs without applying an electric field bias for stabilization of the charge environment. The emission on-time, $\beta=0.35\pm 0.007$, is similar to what is seen in GaAs/AlGaAs QDs under resonant excitation⁴⁰ and reasonably better than GaAs/AlGaAs QDs under quasi-resonant excitation,³⁹ while the blinking time scale $\tau_{Blink}=26.2\pm 1.1$ ns is also similar to the GaAs/AlGaAs QDs.³⁹ Fig. 4c shows the second-order autocorrelation trace of the X^* emission line under ES excitation. The result from the fit is quite similar to the LO phonon assisted excitation for τ_{Blink} , but a slightly larger emission on-time with $\beta=0.44\pm 0.01$ is revealed and no reliable fit result is achieved for $g^{(2)}(0)$.

The correlation time τ_{Corr} defines the width of the antibunching dip at zero-delay. In the simplest case of an adiabatic two-level system, it would be determined by the spontaneous radiative lifetime of the emitter. However, in the case of quasi-resonant excitation, the value of τ_{Corr} may additionally include the component of temporal delay arising from the thermalization process involved in the spontaneous radiative decay from the X^* state. This is particularly the case for the ES excitation, which is better described as a three-level system. For LO phonon assisted excitation we get $\tau_{Corr}=0.84\pm 0.05$ ns, while for ES excitation it is slightly slower with $\tau_{Corr}=0.98\pm 0.08$ ns. These values are somewhat larger than 0.32 ns reported for weakly confined GaAs/AlGaAs QDs,³⁹ but of a similar magnitude to typical radiative lifetimes of radiatively efficient systems like In(Ga)As/GaAs QDs emitting at 920 nm⁴¹ and InAs/InGaAs QDs emitting at 1550 nm.¹⁰ The true radiative lifetimes of the InGaSb/AlGaSb QDs will be assessed in our future work using a pulsed semiconductor laser, which is currently under development.

Fig. 4: Single-photon emission



a Single-QD emission spectrum obtained with $4.5 \mu\text{W}$ LO phonon assisted excitation. The plot shows spectrum for excitation with laser only and for two-color excitation, where a 950 nm LED was added for tuning the charge distribution in the AlGaSb barrier. The LED power density was set to 200 W/m^2 , which was low enough not to produce detectable emission when the laser was switched off. **b** Second-order autocorrelation trace of the X^* line with LO phonon assisted two-color excitation.³⁵ **c** Second-order autocorrelation trace of the X^* line with ES excitation. A two-level model was fitted to the autocorrelation traces to obtain the physical parameters of quantifying photon antibunching and spectral blinking.³⁹ The insets in **b** and **c** show a zoomed in view of the zero-delay region.

Discussion

We have introduced InGaSb/AlGaSb QDs formed by filling droplet-etched nanoholes as a new single-photon source emitting in the 1500 nm wavelength range. A compact frequency-tunable semiconductor laser is utilized for PLE spectroscopy, which is carried out within the excitation wavelength range covering both quasi-resonant ES excitation and LO phonon assisted excitation of the QD ground state. By exciting the QD directly, we can eliminate the complex charge dynamics arising from delayed feeding of charge from a reservoir outside the QD, which are present when using above-band excitation of the barrier material. Consequently, we achieve spectrally pure emission predominantly from a single exciton line (X^*) and pure single-photon emission with $g^{(2)}(0)=0.05\pm 0.03$. This is a considerable improvement compared to our previous work with above-band excitation resulting in non-ideal spectral features and $g^{(2)}(0)=0.16$.²⁰ These results compare well with the data collected from GaAs/AlGaAs QDs under similar experimental conditions in terms of single-photon purity, spectral features, and blinking characteristics.^{30,39} The InGaSb/AlGaSb QDs are thus expected to respond well to

application of an electric field bias from a p-i-n diode for charge stabilization, which is known to completely eliminate blinking in GaAs/AlGaAs QDs.^{13,40}

Furthermore, exciting the QD directly enabled us to, for the first time, study the detailed excitonic structure of antimonide QDs grown by filling droplet-etched nanoholes. Directly exciting the QD states allowed for measuring the key physical properties relevant to furthering the development of antimonide QDs for high-quality single and entangled-photon emission in the third telecom window. In particular, the biexciton binding energy $\Delta E_{xx} = -1.4$ meV (-2.6 nm) is large enough to render possible coherent pumping of the biexciton-exciton cascade by two-photon absorption.^{13,40} Moreover, the FSS values obtained from the investigated QDs ranges from 5 to 26 μ V (Fig.3, Fig. S6), with the larger end of the range being more representative of the population. While these values are not small enough for generation of polarization-entangled photons with high fidelity, they are a good starting point for optimization. Since the nanoholes etched in AlGaSb with Al droplets are highly symmetric (Fig. S1 in the Supp. Info), the asymmetry of the electronic structure is most likely a result of either asymmetric filling or piezoelectric asymmetry resulting from the 0.63% lattice-mismatch between the $\text{In}_{0.1}\text{Ga}_{0.9}\text{Sb}$ QD material and the GaSb substrate. It should be noted, however, that the expected lattice strain is an order of magnitude smaller than, for example, in the InAs/GaAs system (7%). Nevertheless, there is viability for reducing the indium content and simultaneously increasing the QD size to reduce the piezoelectric effects while still maintaining emission in the 1500 nm wavelength region. Such a change in the QD structure would shift the resulting energy structure from strong to weak confinement and provide certain benefits such as a faster radiative rate as seen in GaAs/AlGaAs QDs.²⁶

In summary, we revealed fundamental properties of InGaSb/AlGaSb QDs formed by filling droplet-etched nanoholes. The QDs were embedded in a device structure comprising an antimonide-based Bragg reflector and a solid immersion lens for improving photon collection. Exciting the InGaSb/AlGaSb QDs quasi-resonantly with a compact frequency-tunable semiconductor laser allowed us to study their excitonic fine structure with unprecedented detail. Furthermore, directly addressing the energy states of single QDs allowed us to achieve predominant emission from a single exciton line with a low multi-photon emission probability of $g^{(2)}(0) = 0.05 \pm 0.03$. These results represent a major step forward towards the development of antimonide-based QD materials for quantum photonics and application of a wavelength-flexible semiconductor laser platform as an excitation source for deterministic quantum emitters in secure fiber-based quantum networks.

Materials and methods

Sample fabrication

The epitaxial heterostructure shown in figure X was grown by molecular beam epitaxy (MBE). The layer sequence starts with a 400 nm thick lattice matched $\text{In}_{0.1}\text{Ga}_{0.9}\text{Sb}$ layer, which acts as an absorber to minimize unwanted PL emission from the n-GaSb(100) substrate. The absorber is then capped with a protective 2 nm GaSb layer after which a 9.5-pair bottom Bragg reflector mirror is grown with lattice matched $\text{Al}_{0.9}\text{Ga}_{0.1}\text{As}_{0.07}\text{Sb}_{0.93}/\text{Al}_{0.3}\text{Ga}_{0.3}\text{As}_{0.03}\text{Sb}_{0.97}$ pairs. Finally, a 1λ -thick microcavity is grown consisting of two outer $\frac{1}{4}\lambda$ -thick $\text{Al}_{0.3}\text{Ga}_{0.7}\text{As}_{0.03}\text{Sb}_{0.97}$ and two inner $\frac{1}{4}\lambda$ -thick As-free $\text{Al}_{0.3}\text{Ga}_{0.7}\text{Sb}$ pairs. The QDs are placed at the center of the cavity and are formed by Al-droplet mediated nanohole etching on the $\text{Al}_{0.3}\text{Ga}_{0.7}\text{Sb}$ surface and subsequent filling of the nanoholes by 7.2 monolayers (MLs) of $\text{In}_{0.1}\text{Ga}_{0.9}\text{Sb}$. The etching parameters follow those found in our earlier reports.^{12,20} Namely, the droplets are etched at a

temperature of 395 °C under a low Sb-flux of ~0.06 ML/s for 180 s. The geometry of the resulting nanoholes is shown in Fig. S1 in Supp. Info.

A hemispherical LASFN-9 solid immersion lens (SIL) was attached on top of the MBE-grown sample for improving the photon collection efficiency. Numerical simulation of the collection efficiency and the far field patterns of the QD emission are presented in Section 2 of the Supp. Info.

Excitation laser

The excitation laser used in this work is an Optically Pumped Vertical-External-Cavity Surface-Emitting Laser (OP-VECSEL⁴²). VECSELS combine the advantages of external-cavity solid-state disk lasers with those of quantum-well (QW) semiconductor lasers and provide high output power, excellent beam quality, low noise, high spectral purity, and tunable wavelength versatile operation in a compact footprint. Although still perceived as an emerging laser technology, VECSELS have made considerable progress over the last decade^{27,28} and are becoming key building blocks for Atomic, Molecular and Optical (AMO) physics experiments.

The VECSEL used in this work is a first-of-a-kind prototype of a VALO SF system from Vexlum Inc. It includes the VECSEL head, control electronics, and a low-noise chiller. The VECSEL head comprises a semiconductor gain mirror with AlGaInAs quantum wells with photoluminescence centered at 1428 nm at room temperature, an external cavity with 1% output-coupling mirror mounted on a piezo actuator and with ~1 GHz free-spectral range (fsr), and a fiber-coupled 808 nm diode pump laser for carrier excitation. In free-running configuration (i.e. with empty cavity), the laser outputs >3.5 W of output power at around 1460 nm. To allow broadly tunable single-frequency operation between 1400 – 1470 nm, a 3-mm thick BRF is placed inside the laser cavity and further mounted on a rotation mount with resonant piezoelectric motors to enable precise remote control of the BRF rotation angle around its optical axis and thus the laser wavelength. During BRF rotation, a 6 kHz square wave with a 15 V amplitude is applied to the output coupler piezo to force the laser to jump through all cavity modes with 1GHz resolution originating from the cavity fsr. The resulting wavelength tuning range is shown in Fig. S4a.

Optical experiments

The optical experiments were carried out with a setup custom-built around a low-vibration pulse-tube cryostat cooled down to 5 K. A schematic of the complete setup is presented in Fig. S5 (Supp. Info.). The sample was excited with the semiconductor laser described above. An additional 950 nm LED was used as an optional above-band excitation source for two-color excitation. The power density of the LED was estimated as 200 W/m² power measurement at the back aperture of the objective and the area of the field of view. The LED intensity was optimized for X* emission intensity and kept at a level not producing detectable QD emission without the laser. The excitation beams were combined with non-polarizing beam splitters and focused on the sample with a NA=0.81 objective located inside the cryostat. The same objective was used for collecting the emitted photons. A 1470 nm long-pass filter was used for blocking the back-scattered laser beam during luminescence measurements. The polarization of the laser was controlled with a rotatable $\lambda/2$ waveplate. In polarization-dependent measurements of the QD emission, the detection polarization was filtered using a rotatable $\lambda/2$ waveplate and a fixed polarizer. The laser power was controlled with a variable neutral density filter. The rotation neutral density filter, waveplates, and the laser BRF was automated and integrated as a part of the spectral acquisition software.

The luminescence signal was dispersed on a TE-cooled InGaAs array with a 750 mm spectrograph equipped with a 600 l/cm grating. The single-photon counting was carried out

using the secondary output port of the spectrometer. The photons corresponding to a single emission line were coupled into a 100 m long single-mode fiber. The anti-bunching experiment was carried out at the other end of the fiber using a Hanbury-Brown-Twiss configuration consisting of a 50/50 fiber beam splitter and a pair of superconducting nanowire single-photon detectors. The photon statistics were counted using 39 ps bin size. The combined timing resolution of the detectors and the timing electronics is 40 ps.

Acknowledgements

Financial support from the Finnish Research Council project QuantSi (Decision No. 323989), Business Finland co-innovation project QuTI (41739/31/2020), and the Research Council of Finland Flagship Programm PREIN is acknowledged. TH acknowledges financial support from Tampere University Institute of Advanced Study. The authors would like to thank Prof. Robert Fickler, Lea Kopf, and Jaime Moreno Zuleta for their help in the single-photon autocorrelation experiments.

Conflict of interest

Authors declare no conflict of interest.

Supplementary information

Quantum dot and device characterization; Reflector design and extraction efficiency; Laser characterization; Experimental setup; Additional data for polarization-dependency; Power-dependency of excitons.

References

- ¹ Yin, J. et al. Satellite-based entanglement distribution over 1200 kilometers. *Science* **356**, 1140–1144 (2017).
- ² Wang, H. et al. Boson sampling with 20 input photons and a 60-mode interferometer in a 1014-dimensional Hilbert space. *Phys. Rev. Lett.* **123**, 250503 (2019).
- ³ Zhong, H.-S. et al. Quantum computational advantage using photons, *Science* **370**, 1460–1463 (2020).
- ⁴ Peniakov, G. et al. Towards supersensitive optical phase measurement using a deterministic source of entangled multiphoton states. *Phys. Rev. B* **101**, 245406 (2020).
- ⁵ Zahidy, M. et al. Quantum key distribution using deterministic single-photon sources over a field-installed fibre link, *npj Quantum Information* volume **10**, Article number: 2 (2024).
- ⁶ F. B. Basset et al. "Quantum key distribution with entangled photons generated on demand by a quantum dot", *Sci. Adv.* **7**, 6379 (2021).
- ⁷ Bakker, D.L et al. A Best-Path Approach to the Design of a Hybrid Space-Ground Quantum Network with Dynamic Constraints. Preprints 2024, 2024021515. <https://doi.org/10.20944/preprints202402.1515.v1>
- ⁸ Müller, T. et al. A quantum light-emitting diode for the standard telecom window around 1550 nm, *Nature Communications* **9**, 862 (2018).
- ⁹ Musiał, A. et al. InP-based single-photon sources operating at telecom C-band with increased extraction efficiency, *Appl. Phys. Lett.* **118**, 221101 (2021).

- ¹⁰ Paul, M. et al. Single-photon emission at 1.55 μm from MOVPE-grown InAs quantum dots on InGaAs/GaAs metamorphic buffers, *Appl. Phys. Lett.* **11**, 033102 (2017).
- ¹¹ Zeuner, K.D. On-Demand Generation of Entangled Photon Pairs in the Telecom C-Band with InAs Quantum Dots, *ACS Photonics* **8**, 2337 (2021).
- ¹² Chellu, A. et al. Highly uniform GaSb quantum dots with indirect–direct bandgap crossover at telecom range, *APL Mater.* **9**, 051116 (2021)
- ¹³ Zhai, L. et al. Low-noise GaAs quantum dots for quantum photonics, *Nat. Commun.* **11**, 4745 (2020).
- ¹⁴ Keil, R. et al. Solid-state ensemble of highly entangled photon sources at rubidium atomic transitions, *Nat. Commun.* **8**, 15501 (2017)
- ¹⁵ Liu, J. et al. A solid-state source of strongly entangled photon pairs with high brightness and indistinguishability *Nat. Nanotechnol.* **14**, 586 (2019).
- ¹⁶ Huo, Y.H. et al. Ultra-small excitonic fine structure splitting in highly symmetric quantum dots on GaAs (001) substrate *Appl. Phys. Lett.* **102**, 152105 (2013).
- ¹⁷ Huber, D. et al. Highly indistinguishable and strongly entangled photons from symmetric GaAs quantum dots *Nat. Commun.* **8**, 15506 (2017).
- ¹⁸ Schöll, E. Resonance Fluorescence of GaAs Quantum Dots with Near-Unity Photon Indistinguishability, *Nano Lett.* **19**, 2404 (2019).
- ¹⁹ Huber, D. Strain-Tunable GaAs Quantum Dot: A Nearly Dephasing-Free Source of Entangled Photon Pairs on Demand, *Phys. Rev. Lett.* **121**, 033902 (2018).
- ²⁰ Michl, J. et al. Strain-Free GaSb Quantum Dots as Single-Photon Sources in the Telecom S-Band, *Adv Quantum Technol.* **6**, 2300180 (2023).
- ²¹ Huang, S.H. et al. Strain relief by periodic misfit arrays for low defect density GaSb on GaAs *Appl. Phys. Lett.* **88**, 131911 (2006).
- ²² Huang, S.H. et al. Simultaneous interfacial misfit array formation and antiphase domain suppression on miscut silicon substrate, *Appl. Phys. Lett.* **93**, 071102 (2008).
- ²³ Rodriguez, J.B. et al. X-ray diffraction study of GaSb grown by molecular beam epitaxy on silicon substrates *J. Cryst. Growth* **439**, 33 (2016).
- ²⁴ Tournie, E. et al. Mid-infrared III-V semiconductor lasers epitaxially grown on Si substrates, *Light: Science & Applications* **11**, 165 (2022).
- ²⁵ Leguay, L. et al. Unveiling the electronic structure of GaSb/AlGaSb quantum dots emitting in the third telecom window, *Mater. Quantum. Technol.* **4** 015401 (2024).
- ²⁶ Reindl, M. et al. Highly indistinguishable single photons from incoherently excited quantum dots, *Phys. Rev. B* **100**, 155420 (2019).
- ²⁷ Burd, S.C. et al. VECSEL systems for quantum information processing with trapped beryllium ions, *Journal of the Optical Society of America B* **40**, 773-781, (2023).
- ²⁸ Burd, S.C. VECSEL systems for the generation and manipulation of trapped magnesium ions, *Optica* **3**, 1294-1299 (2016).
- ²⁹ Penttinen, J.-P. et al. Sub-Hz single-frequency VECSELs for optical clocks. *Quantum Sensing, Imaging, and Precision Metrology II.* (p. PC1291207) SPIE, 2024.
- ³⁰ Reindl, M. Highly indistinguishable single photons from incoherently excited quantum dots, *Phys. Rev. B* **100**, 155420 (2019).
- ³¹ Pooley, M.A. Controlled-NOT gate operating with single photons, *Appl. Phys. Lett.* **100**, 211103 (2012).
- ³² Ferrini, R. et al. Phonon response of $\text{Al}_x\text{Ga}_{1-x}\text{Sb}/\text{GaSb}$ epitaxial layers by Fourier-transform infrared-reflectance and Raman spectroscopies, *Phys. Rev. B* **56**, 7549 (1997).
- ³³ Li Hui et al. "Defect properties of as-grown and electron-irradiated Te-doped GaSb studied by positron annihilation" *Semicond. Sci. Technol.* **26** 075016 (2011).

- ³⁴ Kujala, J. et al. Native point defects in GaSb J. Appl. Phys. **116**, 143508 (2014)
- ³⁵ Gazzano, O. et al. Bright solid-state sources of indistinguishable single photons. *Nat. Commun.* **4**, 1425 (2013).
- ³⁶ Graf, A. et al. Excitonic states in GaAs quantum dots fabricated by local droplet etching, Phys. Rev. B **89**, 115314 (2014).
- ³⁷ Rodt, S. et al. Repulsive exciton-exciton interaction in quantum dots, Phys. Rev. B **68**, 035331 (2003).
- ³⁸ Gazzano, O. et al. Bright solid-state sources of indistinguishable single photons. *Nat. Commun.* **4**, 1425 (2013).
- ³⁹ Hopfmann, C. et al. Heralded preparation of spin qubits in droplet-etched GaAs quantum dots using quasiresonant excitation, Phys. Rev. B **104**, 075301 (2021).
- ⁴⁰ Schimpf, C. Entanglement-based quantum key distribution with a blinking-free quantum dot operated at a temperature up to 20 K, *Advanced Photonics* **3**, 065001 (2021).
- ⁴¹ Stobbe, S. et al. Frequency dependence of the radiative decay rate of excitons in self-assembled quantum dots: Experiment and theory. *PHYSICAL REVIEW B* **80**, 155307 (2009)
- ⁴² Guina, M. et al. "Optically pumped VECSELs: review of technology and progress" *J. Phys. D: Appl. Phys.* **50**, 383001 (2017).

Supplementary information for Telecom wavelength single-photon source based on InGaSb/AlGaSb quantum dot technology

Teemu Hakkarainen,^{1,2*} Joonas Hilska,¹ Arttu Hietalahti,³ Sanna Ranta,¹ Markus Peil,¹ Emmi Kantola,³ Abhiroop Chellu,¹ Efsane Sen,¹ Jussi-Pekka Penttinen,³ Mircea Guina¹

¹ Optoelectronics Research Centre, Physics Unit, Tampere University, FI-33720 Tampere, Finland

² Institute for Advanced Study, Tampere University, FI-33100 Tampere Finland

³ VEXLUM Oy, FI-33710 Tampere, Finland

*Corresponding author: teemu.hakkarainen@tuni.fi

Section 1 quantum dot and device characterization

The InGaSb/AlGaSb quantum dots (QDs) were fabricated by filling InGaSb inside nanoholes etched by Al droplets on an AlGaSb surface. A topographic image of the AlGaSb surface containing nanoholes before filling them with InGaSb was captured by atomic force microscopy (AFM; Bruker Dimension Icon) and is presented in Fig. S1a. Line profiles of a single nanohole taken along two orthogonal in-plane crystal directions reveal a nanohole depth of ~16 nm.

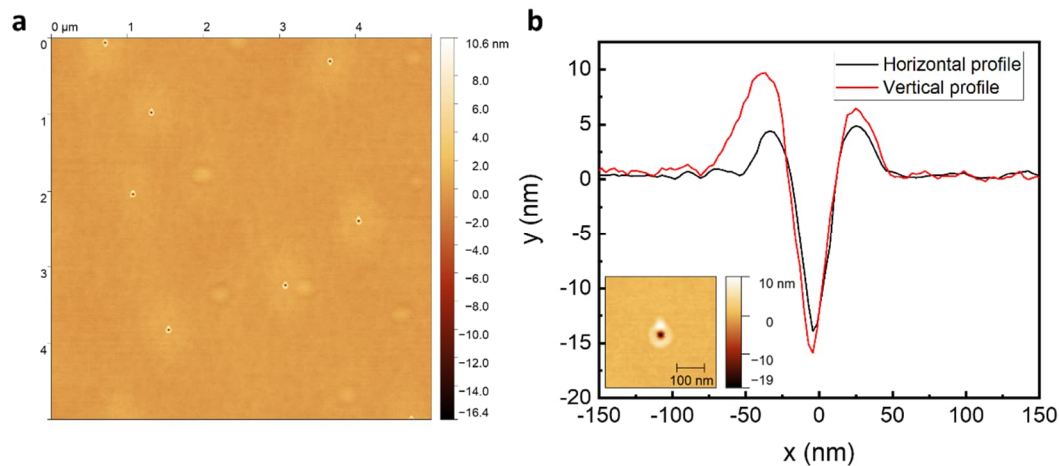


Fig. S1. **a** AFM micrograph of nanoholes etched in AlGaSb with Al droplets. The density of the nanoholes is $3.6 \times 10^7 \text{ cm}^{-2}$. **b** Cross-sectional profiles of a single nanohole reveal a nanohole depth of ~16 nm.

Photoluminescence (PL) spectra collected from a large ensemble of QDs embedded in a planar AlGaSb layer A FWHM of ~6 meV (11 nm) measured for the PL emission peak of the QD ensemble attests to the remarkable homogeneity in the size of the fabricated QDs. It should be noted that this experiment was carried out with above-band excitation which triggers emission from a collection of excitonic transitions within each QD. Therefore, any QD-to-QD variation of a specific exciton line is expected to be considerably smaller due to the excellent homogeneity of the QD dimensions. As shown in Fig. S2b, the device structure including the DBR and the InAsSb absorber increases the QD peak intensity and suppresses the GaSb

substrate emission. The DBR cavity was designed to match the QD emission at 1500 nm, as shown by the reflection spectrum in Fig. S2c.

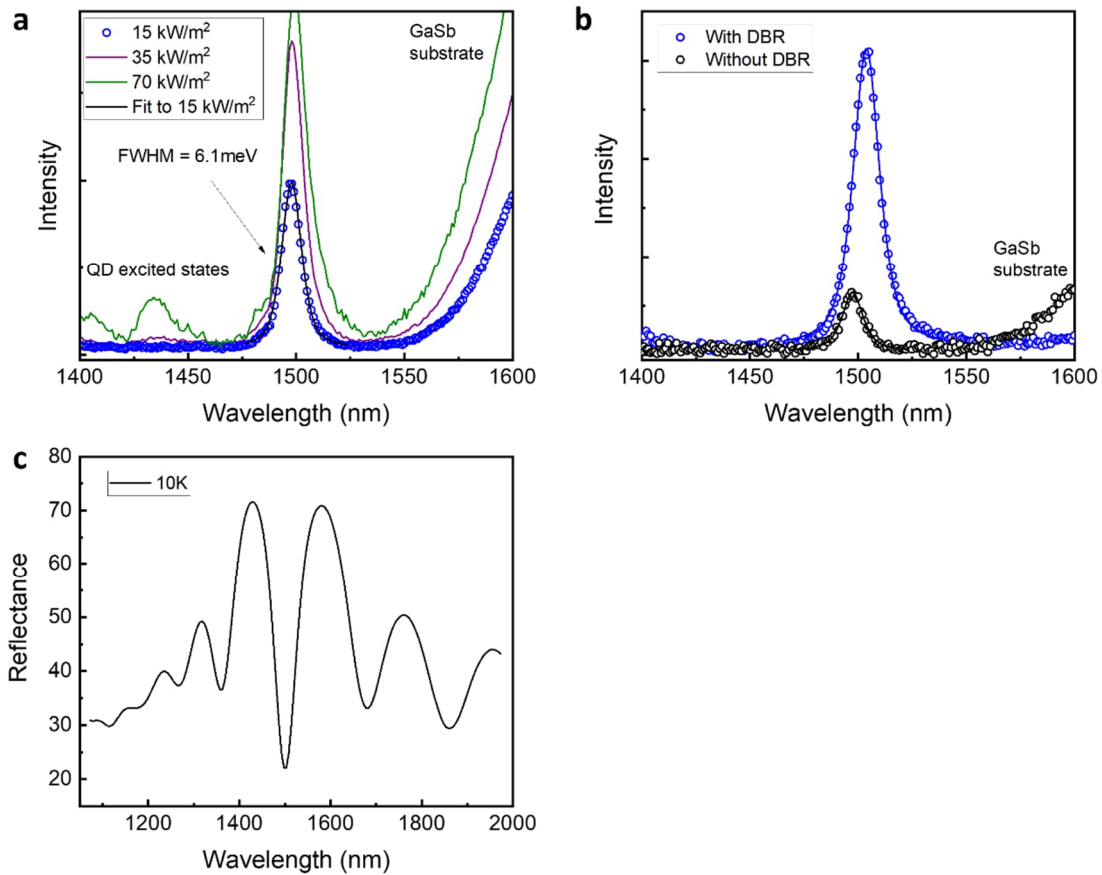


Fig. S2. **a** Photoluminescence emission from an ensemble of InGaSb QDs without a DBR back-reflector collected from an area of several mm². Measurement was carried out with 532 nm excitation with different power levels to identify the QD excited states. The QD homogeneity was estimated from the QD ground state peak width below saturation power. **b** Improvement of emission intensity and suppression of GaSb substrate emission after adding the DBR back-reflector and the InAsSb absorber. **c** reflectance spectrum of the DBR cavity structure showing resonance of the cavity dip with the QD emission wavelength.

Section 2 Reflector design and extraction efficiency

Collection efficiency of QD emission from within a planar AlGaSb layer using an objective with NA=0.81 is only 1.2% due to the high refractive index of the antimonide materials. Therefore, a DBR back-reflector and a solid immersion lens were included for improving the collection of the emitted photons. The QDs were placed in the middle of an AlGaSb λ -cavity and the DBR consisted of 9.5 pairs of Al_{0.9}GaAsSb/Al_{0.3}GaAsSb $\lambda/4$ layers. The design wavelength was 1500 nm, which matches with the QD ground state. A numerical simulation of the full device structure is presented in Fig. S3, which shows a collection efficiency of 16% at the design wavelength for NA=0.81. Further improvement of the collection efficiency could be achieved by red-shifting the targeted design wavelength for the QD emission. However, this would come at the expense of the far-field pattern becoming less Gaussian which would be detrimental for coupling the photons into a single-mode fiber necessary for the measurement of single-photon statistics.

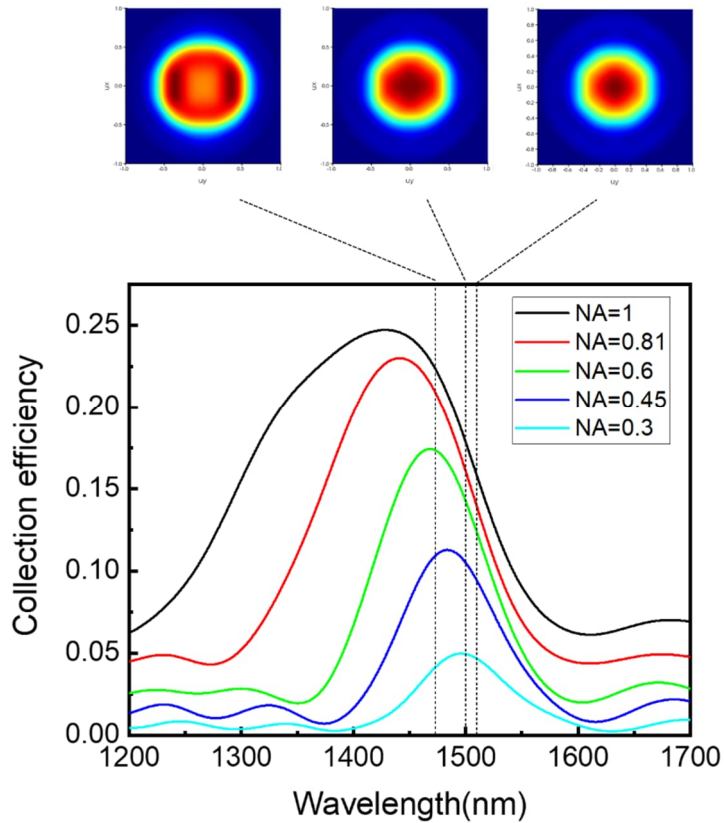


Fig. S3. FDTD simulation of the photon collection efficiency for the device structure including DBR and a solid immersion lens. Far-field patterns are shown for three wavelengths around the design wavelength of 1500 nm.

Section 3 laser characterization

Fig. S4 presents the characteristics of the excitation laser for wavelength-tuning. The full lasing range is shown in Fig. S4a as measured directly from the laser output. The beam was then coupled into a single-mode fiber in order to transport it to the optical setup. The power of the laser during wavelength scans was normalized by adjusting the pump power, with feedback coming from a photodiode (see Fig. S5). The decrease of the laser power with increasing BRF angle in Fig. S4b is because of the wavelength response of the fiber beam splitter which is designed for a narrow band centered around 1550 nm. A flat power response can be achieved using a splitter optimized for the operation wavelength of the laser.

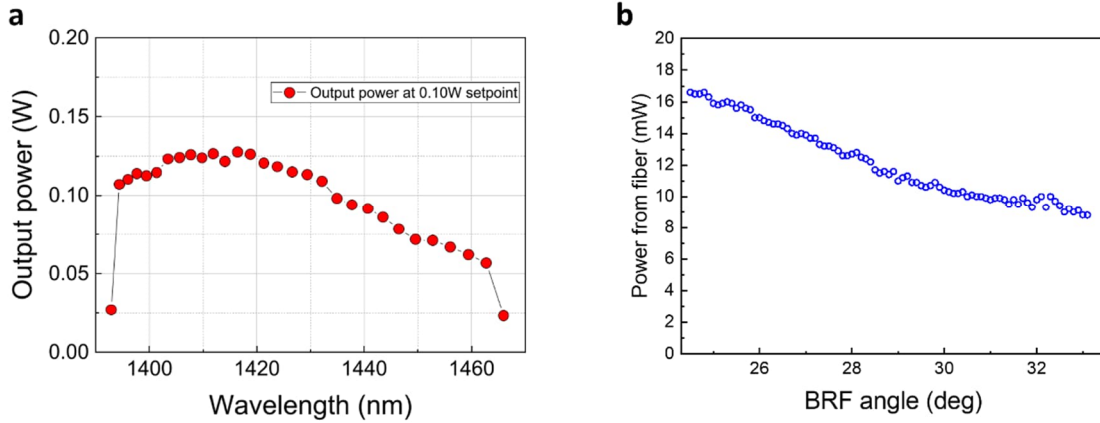


Fig. S4. a The full tuning range of the laser as measured directly from the laser output beam. **b** Stabilized laser power measured from the end of the fiber (after attenuation) for a wavelength scan carried out by rotating the BRF. The power stabilization was achieved by adjusting the pump power based on the feedback from a fiber-coupled photodiode (PD in Fig. S5) sampling the laser intensity in the fiber.

Section 4 experimental setup

Figure S5 presents the optical setup used in the experiments. The polarization of the laser and detection were controlled with a waveplate (WP) and a WP and polarizer (POL), respectively. The laser power was controlled with a variable neutral density filter (ND). An additional 950 nm LED was used as a weak above-band light source for two-color excitation. The beams were combined with non-polarizing beam splitters (BS) and focused on a sample with NA=0.81 microscope objective located inside the cryostat. The same objective was used for collecting the photons emitted by the QD. The luminescence signal was filtered with a long-pass filter (LP) and dispersed on a TE-cooled InGaAs array with a 750 mm spectrometer equipped with a 600 lines/mm grating. The single-photon counting was carried out via the secondary output port of the spectrometer. The photons corresponding to a single emission line from the QD were coupled into a 100 m long single-mode fiber. The antibunching experiment was carried out at the other end of the fiber using a Hanbury-Brown-Twiss configuration consisting of a 50/50 fiber beam splitter (FBS) and a pair of superconducting nanowire single-photon detectors (SNSPDs).

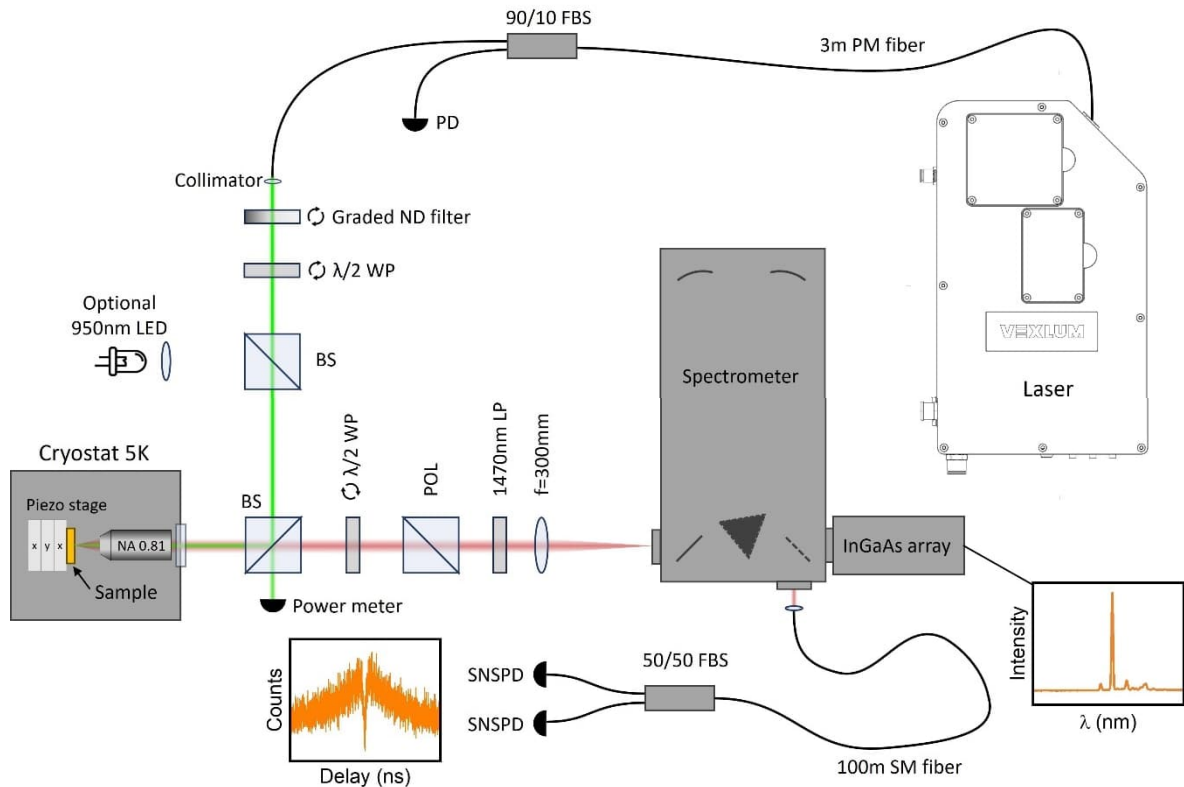


Fig. S5. Schematic of the experimental setup used for spectroscopy and single-photon autocorrelation.

Section 5 Polarization-dependency of excitons

In addition to the QD discussed in the main text (QD1), additional polarization-resolved spectra were collected from four other QDs (referred to as QD2-QD5). As shown in Fig. S6a for QD2, the investigated QDs show basic characteristics similar to QD1, including XX (X) emission at slightly shorter (longer) wavelength than X^* . The fine structure splitting (FSS) ranges from 5 μeV (QD4) to 26 μeV (QD3), with values above 20 μeV being most representative for the investigated sample based on the available statistics. It is also worth noting that the orientation of the FSS is consistently along one of the [110] crystal directions, which suggests that it is resulting from asymmetry of the nanohole shape or filling or piezoelectric asymmetry caused by the strain of $\text{In}_{10}\text{Ga}_{90}\text{Sb}$ which has 0.63% lattice-mismatch with respect to the GaSb substrate.

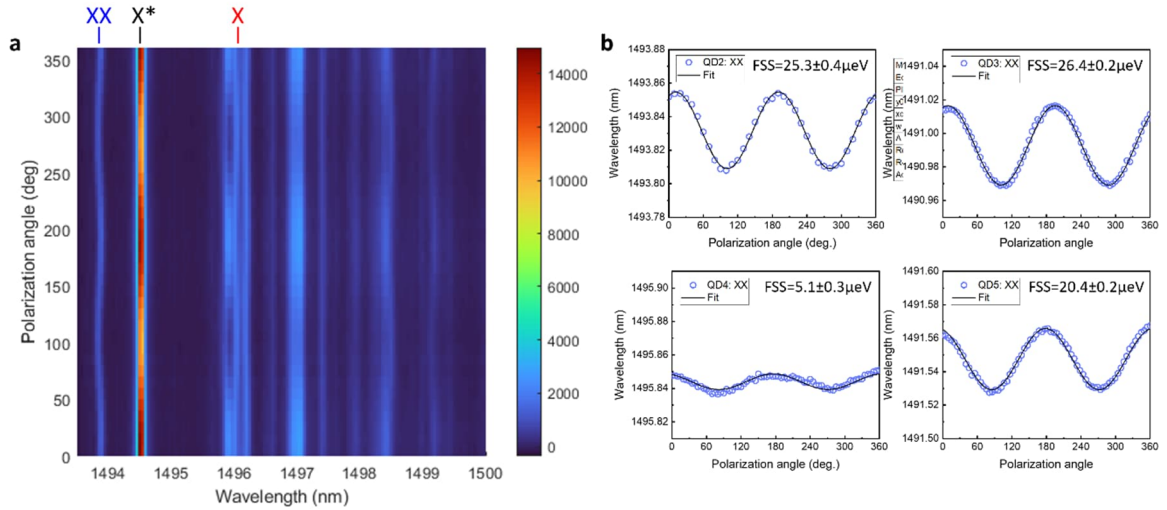


Fig. S6. Polarization-dependent data for four additional QDs. **a** Polarization-dependent spectra for QD2. **b** Biexciton peak position as a function of polarization angle and estimated FSS value for QD2-QD5. QD1 is presented in the main text.

Section 6 Power-dependency of excitons

The various individual exciton lines were identified by analyzing their behavior as a function of detection polarization (in main text) and excitation power. Fig. S7 shows the power-dependent data for the QD discussed in the main text (QD1). The power-dependent spectra were measured with ES excitation scheme first by using only the laser as an excitation source. Then the experiment was repeated using the two-color excitation scheme¹ with a 950 nm LED acting as additional excitation source for stabilizing the charge environment around the QD by above-band generation of electron-hole pairs in the AlGaSb matrix. The power density of the LED was set to a level low enough to not produce detectable excitonic emission in the absence of the laser excitation. The peak intensity data for the two scenarios are presented in Fig. S7b and c. Complex charge dynamics are observed in both cases, but clear power-law-behavior $I_{exciton} \propto P_{laser}^{\alpha}$ is observed over certain laser power ranges. The neutral exciton (X) and biexciton (XX), i.e. the lines exhibiting FSS in the polarization-resolved data, can be identified with X having $\alpha \approx 1$ and XX having $\alpha \approx 2$. The dominant exciton X* line is identified as a trion with $\alpha \approx 1.5$ and no FSS. At low to moderate excitation powers we observe also X_c, for which $\alpha \approx 1.5$ and no FSS is observed in the polarization-dependent data. X* and X_c are most probably trions with opposite charges. Given the type of native point defects in GaSb materials^{2,3}, it is likely that the dominant X* line is a positively charged trion and X_c the negatively charged counterpart. At the higher power range, we observe also a group of lines related to multiply-charged excitons and charged biexcitons⁴, which were not investigated in detail.

The competition between neutral, positively, and negatively charged excitons suggests that the InGaSb/AlGaSb QDs would benefit from being embedded in a diode structure which allows stabilization and control of the charge state as shown for the GaAs/AlGaAs QD system⁵. As seen from the intensities of X* and X_c in Fig. S7b and c, two-color excitation provides some control of the charge state by shifting the dynamics in favor of the dominant X* line. This feature was used for achieving higher X* intensity with the LO phonon assisted excitation scheme (Fig. 4 in the main text).

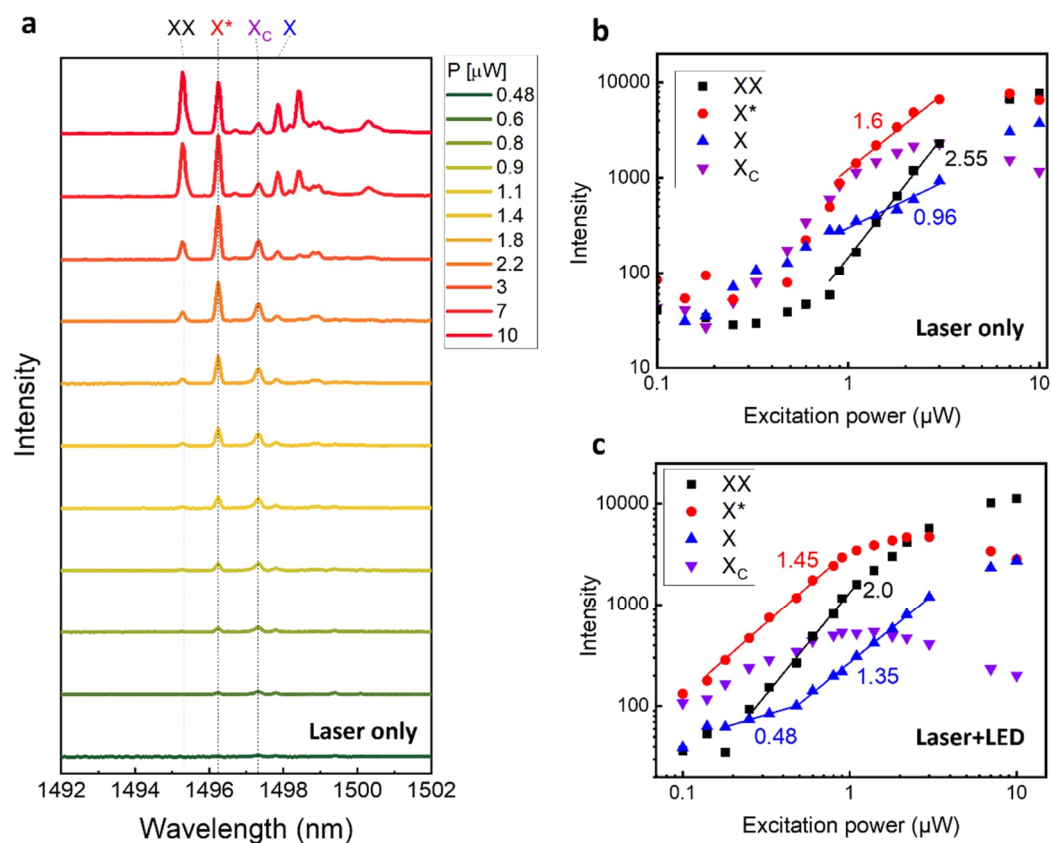


Fig. S7. Power-dependent spectra with excited state excitation for the QD presented in the main text (QD1). **a** PL spectra for different excitation powers when excited with the laser only (vertically offset for visual purposes). **b** and **c** show the intensities of exciton lines as a function of laser power for excitation with laser only and excitation with the laser accompanied by a 950 nm LED (1400 W/m^2), respectively.

References

- ¹ Gazzano, O. et al. Bright solid-state sources of indistinguishable single photons. *Nat. Commun.* **4**, 1425 (2013).
- ² Li Hui et al. "Defect properties of as-grown and electron-irradiated Te-doped GaSb studied by positron annihilation" *Semicond. Sci. Technol.* **26** 075016 (2011).
- ³ Kujala, J. et al. Native point defects in GaSb *J. Appl. Phys.* **116**, 143508 (2014)
- ⁴ Ediger, M., Bester, G., Badolato, A. et al. Peculiar many-body effects revealed in the spectroscopy of highly charged quantum dots. *Nature Phys* **3**, 774–779 (2007).
- ⁵ Zhai, L., Löbl, M.C., Nguyen, G.N. et al. Low-noise GaAs quantum dots for quantum photonics. *Nat Commun* **11**, 4745 (2020).